Posted on 11 Nov 2022 — The copyright holder is the author/funder. All rights reserved. No reuse without permission. — https://doi.org/10.22541/au.166817987.71310189/v1 — This a preprint and has not been peer reviewed. Data may be preliminary.

High Mobility Hafnium and Hydrogen Co-Doped Indium Oxide Transparent Conductive Films and Application in High Efficiency Silicon Heterojunction Solar Cell

Jiacheng Shang[1], Qi Wang[2], Shuai Zhou[3], Wanwu Guo[4], Rong Zhou[1], Yuqin Zhou[1], and Fengzhen Liu[1]

[1]University of the Chinese Academy of Sciences
[2]Suzhou Maxwell Technologies Co Ltd
[3]Weiqiao-UCAS Science and Technology Park
[4]Jetion Solar (China) Co Ltd

November 11, 2022

Abstract

In this work, high quality hafnium and hydrogen co-doped In_2O_3 (IHfO:H) transparent conductive films are developed via a reactive plasma deposition (RPD) technique followed by air atmosphere annealing. Crystallinity, valence states, and opto-electronic properties of the IHfO:H films under different H_2 concentration (0-1.5 %) and different annealing temperature (100-250 °C) are systematically investigated. The effects of hydrogen doping and annealing temperature on the properties of the IHfO:H films are discussed. The high average transmittances (400-800 nm: 87.92 %; 800-2300 nm: 86.68 %), a sheet resistance of 27.53 Ω/, and a Hall mobility of 102.92 $cm^2V^{-1}s^{-1}$ are achieved on the optimized IHfO:H thin film fabricated using 0.8 % H_2 concentration with a 200 °C annealing temperature. Finally, the IHfO:H films are applied to the bifacial silicon heterojunction (SHJ) solar cells to serve as the front-side transparent electrode. The significant improvement in the long wavelength spectral response compared to the control SHJ device with an indium tin oxide (ITO) front-side transparent electrode leads to an increase of about 0.3 % in the efficiency and an efficiency of over 25 % is achieved on the SHJ solar cell with an IHfO:H front-side transparent electrode.

1 Introduction

In recent decades, silicon heterojunction (SHJ) solar cells based on intrinsic amorphous silicon passivation layers and doped amorphous or microcrystalline silicon carrier selective layers have attracted more and more attention due to their advantages of high efficiency, weak light attenuation and low temperature coefficient.[1-2]The SHJ technology has succeeded in bringing the conversion efficiency of monocrystalline silicon solar cells to over 26 %.[3]Due to the relatively low carrier diffusion length of doped amorphous or microcrystalline silicon films, transparent conductive oxide (TCO) electrodes are essential for achieving efficient lateral carrier collection in the SHJ solar cells. High quality TCO layers with good optical and electrical properties are crucial for SHJ solar cells to realize high fill factor (FF) and high short-circuit current density (J_{sc}). Indium tin oxide (ITO) thin film is widely used in the industrial production of SHJ solar cells because of its high electrical conductivity. So far, in many reported high-efficiency SHJ solar cells, the ITO films were utilized as the front or bifacial transparent conductive electrodes.[4-5] Different deposition techniques, including direct current (DC) or radio frequency (RF) sputtering,[6] thermal[7] or electron beam evaporation,[8] plasma-enhanced reactive thermal evaporation,[9] and pulsed laser deposition,[10] etc., have been successfully employed to deposit ITO films with high conductivity. However, the Hall mobility of the ITO films prepared by these methods mentioned above is typically below 50 $cm^2V^{-1}s^{-1}$. The high conductivity characteristic of

Posted on 11 Nov 2022 — The copyright holder is the author/funder. All rights reserved. No reuse without permission. — https://doi.org/10.22541/au.166817987.71310189/v1 — This a preprint and has not been peer reviewed. Data may be preliminary.

ITO mainly benefits from the high carrier concentration (usually in the order of $10^{21}cm^{-3}$) which causes serious parasitic absorption in the near-infrared (NIR) region and limits the short-circuit current density of the SHJ solar cells.[11] To explore TCO films with both high transmittance and high mobility, so as to improve the J_{sc} to catch up with the Tunnel Oxide Passivated Contact (TOPCon) solar cells, is one of the main research directions of the high efficiency SHJ solar cells.

According to the literature, the relatively low mobility of ITO is mainly related to the low doping efficiency of tin.[12]Substitutional doping of Sn^{4+} with smaller ionic radius may cause lattice distortion in ITO and, as a less efficient dopant,[13] relatively high doping concentration of tin impurities is required to achieve low resistivity.[14]To obtain TCO films with high mobility and low carrier concentration, various metal elements with higher ionic valence or more matched ionic radius with In^{3+}, such as W,[15]Mo,[16] Ce[17] and Hf,[18] etc., were proposed to replace Sn as the dopant elements of indium oxide films to reduce the impurity concentration without compromising film conductivity. Among them, indium oxide doped with Hf (IHfO) presents excellent opto-electronic properties and great application potential. A Hall mobility of 79.6 $cm^2V^{-1}s^{-1}$, a carrier concentration of $5.04\times10^{20}cm^{-3}$ and a resistivity of $3.76\times10^{-4}\Omega\cdot cm$ were achieved on IHfO thin film grown by magnetron sputtering technique.[19] The IHfO films have been successfully applied on amorphous silicon germanium thin film solar cells and SHJ solar cells and obtained conversion efficiencies of 8.3% and 19.08%, respectively.[18-19]

In recent years, reactive plasma deposition (RPD) technology, also named as hollow cathode discharge deposition, has been used to prepare TCO films and has received wide attention of the researchers in the field of heterojunction solar cells.[20] During the RPD process, the substrate is not directly exposed to the plasma and the damage related to the ion bombardment is greatly reduced.[20]Thereby, RPD is considered to be a suitable technique for the devices such as heterojunction solar cells with extremely high-quality interface requirements. Furthermore, RPD is actually an ion-plating method working in the arc discharge plasma regime with low-voltage and high-current. The high ionization yield is conducive to promote the gas phase reaction and improve the opto-electronic properties of the grown TCO films. Previously, some TCO films including ZnO,[21] Ce-doped In_2O_3 (ICO),[22] W-doped In_2O_3 (IWO)[23] and W and Ti co-doped In_2O_3(IWTO)[24] have been successfully grown by RPD and have exhibited excellent opto-electronic properties. However, more research work is still needed in IHfO films prepared using RPD technique and application of IHfO films in high efficiency SHJ solar cells is also expected.

In this work, hydrogen doped IHfO thin films (IHfO:H) were prepared by RPD technique. The effects of hydrogen concentration and post-annealing temperature on the crystallinity, opto-electronic properties, and valence states of the IHfO:H thin films were investigated. Under the conditions of H_2 concentration of 0.8 % and post-annealing temperature of 200 °C, the IHfO:H films with the best comprehensive properties were obtained. The IHfO:H thin film prepared under the optimized condition was applied to the bifacial SHJ solar cell as the front TCO layer and a conversion efficiency of more than 25 % has been achieved.

2 Experimental details

2.1 Preparation of IHfO:H thin films:

IHfO:H thin films were deposited on glass and polished silicon wafers by RPD to investigate their microstructure, morphology, opto-electronic properties, and chemical valence states. HfO_2-doped In_2O_3 particles (4 wt % HfO_2, 99.99 % purity) were used as the target. High-purity argon with the fixed flow rate of 30 sccm and argon-hydrogen mixture (30 % hydrogen) with the varied flow rate between 0 and 1.5 sccm were used as the working gas. The chamber pressure was controlled to be at 0.4-0.5 Pa and the working current of power was set at 60 A. The thicknesses of all the IHfO:H films are around 100 nm (±5 nm). The post-annealing process was carried out in air with the annealing time of 20 minutes and the annealing temperature of 50-250 °C.

2.2 Fabrication of SHJ solar cells:

The n-type Cz crystalline silicon wafers with the thickness of 170 μm and resistivity of 1 Ω·cm were used

Posted on 11 Nov 2022 — The copyright holder is the author/funder. All rights reserved. No reuse without permission. — https://doi.org/10.22541/au.166817987.71310189/v1 — This a preprint and has not been peer reviewed. Data may be preliminary.

as the substrates. Alkaline texturing, chemically polishing and RCA cleaning procedures were performed prior to the fabrication of the SHJ solar cells. The SHJ solar cells adopt a bifacial light incident structure of Ag grids/IHfO:H/μc-Si:H(n^+)/a-Si:H(i)/n type c-Si/ a-Si:H(i)/a-Si:H(p^+)/ITO/Ag grids, as specifically shown in Figure 1. The intrinsic hydrogenated amorphous silicon (a-Si:H(i)) passivation layers with the thickness of 7 nm were deposited on both sides of the n-type crystalline silicon by plasma enhanced chemical vapor deposition (PECVD). A 10 nm p-type amorphous silicon (a-Si:H(p^+)) layer and a 7 nm n-type microcrystalline silicon μc-Si:H(n^+) layer, also deposited by PECVD, serve as the hole transport layer (emitter) and electron transport layer, respectively. A 100 nm IHfO:H film, as both the transparent conductive layer and the antireflection layer, was prepared by RPD. A 70 nm ITO film was prepared by the magnetron sputtering method on the back side of the SHJ solar cells. The silver grids on both sides of the device were prepared by screen printing technology. After electrode printing was completed, the whole solar cells were annealed in air at a temperature of 200 °C for 20 minutes.

2.3 Characterization:

The thickness of the IHfO:H films was measured by a step profiler (Bruker DektakXT). X-ray diffraction (Rigaku Smartlab SE) measurement was carried out to analyze the crystal structure of the IHfO:H thin films using a Cu-Kα radiation source ($\lambda = 1.5405$ Å), scanned in 2ϑ mode, with the diffraction angles ranging from 10 to 80 °. The square resistance of the IHfO:H films was measured by the four-probe method, while the carrier concentration and Hall mobility were obtained from the Hall measurement (PSAICSwin Hall 8686). A UV-Vis-NIR spectrophotometer (Perkin-Elmer Labmda 750) was used to obtain the optical transmission spectra of the films. The chemical state characterization of the IHfO:H films was determined using X-ray photoelectron spectroscopy (XPS, Kratos Axis Supra+). In order to exclude the effect of adsorbed air on the surface, all samples were etched with Ar ion beam for 1 minute before the XPS measurement. The light current-voltage (I-V) curves of the solar cells were obtained using a solar simulator under standard conditions (100 mW/cm^2, AM 1.5 G, 25 °C). The external quantum efficiency (EQE, BENTHAM INSTRUMENT PVE300-IVT) was measured to study the spectral response of the solar cells.

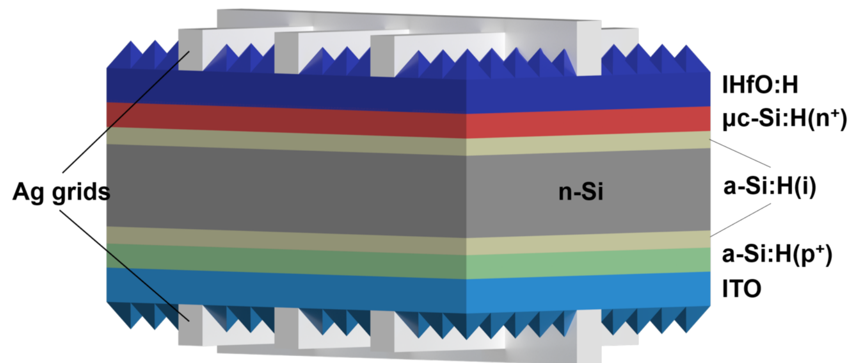

Figure 1 Schematic of the bifacial SHJ solar cells based on n-type monocrystalline silicon wafers.

3 Results and discussion

3.1 Effect of hydrogen concentration on the IHfO:H thin films

Hydrogen doping has been proved to be an effective strategy to modify the performance of the TCO films, such as reducing the square resistance and improving the mobility, by influencing the crystallinity, forming shallow donor states, and passivating the structural defects.[25-27] We investigated the effects of hydrogen doping on the IHfO:H films by varying the H_2concentrations (gas flow ratio of hydrogen to argon: 0 %, 0.5

%, 0.8 %, 1.2 % and 1.5 %) during the deposition process. Referring to the fabrication process of traditional SHJ solar cells, the series of IHfO:H films were all annealed at 200 °C in air for 20 minutes.

Figure 2 shows the XRD patterns of the IHfO:H films with different hydrogen concentrations after annealing at 200 °C. According to the standard comparison card (JCPDS No.06-0416), the diffraction peaks of (211), (222), (332), and (444) belonging to the cubic bixbyite polycrystalline structure of In_2O_3 are observed. The absence of diffraction peaks for HfO_2indicates that substitutional doping (Hf^{4+} replacing In^{3+}) forms a solid solution in which HfO_2 was dissolved into the In_2O_3 lattice during the film growth process.[28] The intensity of the diffraction peak (222) in all samples is much higher than that of the other peaks, which indicates that (222) is the preferential crystallization direction. We calculated the average grain size D of the IHfO:H films corresponding to the full width at half maximum (FWHM) of the (222) diffraction peak according to the Scherrer formula,[19] as included in Figure 2.

It can be seen that the average grain sizes of all the samples are in the range of 50±5 nm, which implies that the H_2concentration hardly affects the crystallinity of the films. Annealing can greatly improve the crystallinity of the IHfO:H films, thus weakening the effect of hydrogen doping on the crystallinity of the films, as will be discussed below.

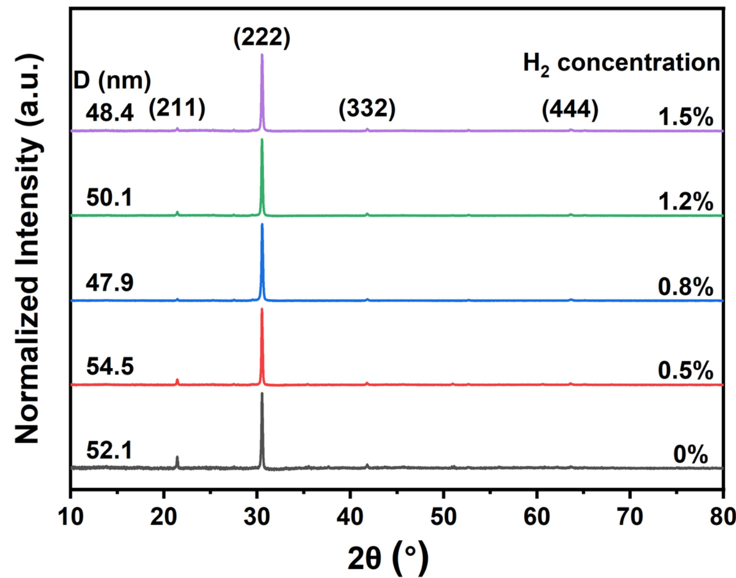

Figure 2 Normalized XRD patterns of the IHfO:H films with 0 %, 0.5 %, 0.8 %, 1.2 % and 1.5 % H_2 concentration after post-annealing at 200 .

The electrical properties of the IHfO:H films prepared with different hydrogen concentrations are shown in Figure 3. It can be seen that the sheet resistance of the IHfO:H films decreases first and then increases as the increase of the hydrogen concentration, reaching a minimum of 27.53 Ω/ at a hydrogen concentration of 0.8 %. For TCO films with the same thickness, the sheet resistance is mainly affected by the mobility and the carrier concentration. In order to clarify the influence mechanism of the hydrogen concentration on the sheet resistance of the IHfO:H films, the Hall mobility and the carrier concentration of the IHfO:H films were studied, also depicted in Figure 3.

Posted on 11 Nov 2022 — The copyright holder is the author/funder. All rights reserved. No reuse without permission. — https://doi.org/10.22541/au.166817987.71310189/v1 — This a preprint and has not been peer reviewed. Data may be preliminary.

Posted on 11 Nov 2022 — The copyright holder is the author/funder. All rights reserved. No reuse without permission. — https://doi.org/10.22541/au.166817987.71310189/v1 — This a preprint and has not been peer reviewed. Data may be preliminary.

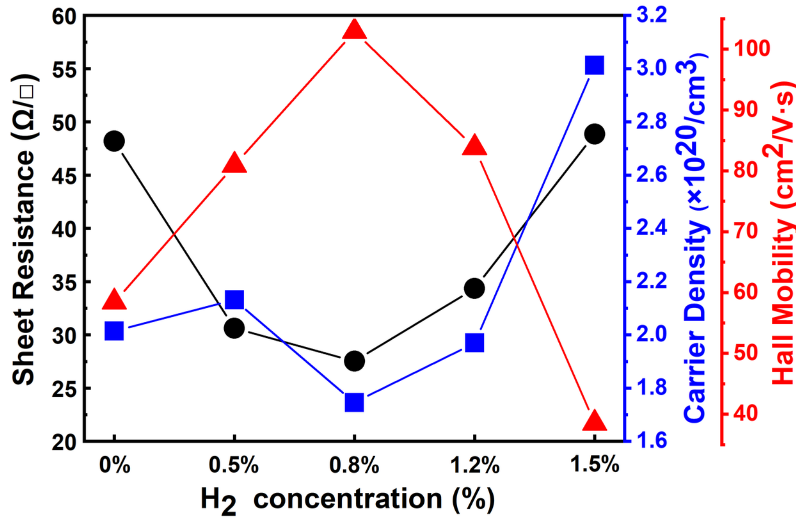

Figure 3 Sheet resistance, carrier concentration and Hall mobility of the IHfO:H films prepared with 0 %, 0.5 %, 0.8 %, 1.2 % and 1.5 % H_2 concentration after post-annealing at 200 .

The Hall mobility increases at first and then decreases with increasing the H_2 concentration, reaching a maximum of 102.92 $cm^2V^{-1}s^{-1}$at a H_2 concentration of 0.8 %. Three carrier scattering mechanisms including acoustical phonon scattering, ionized impurity scattering, and grain boundary scattering are generally considered as the main mechanisms to affect the mobility of the TCO films.[29] Considering that the electrical properties were measured at the room temperature and no significant crystallinity difference can be determined (as Figure 2 shows), phonon scattering and grain boundary scattering should not be the main factors that cause the mobility difference in the IHfO:H films with different H_2 concentrations. Therefore, it can be inferred that the variation of Hall mobility is mainly caused by the difference in the intensity of ionized impurity scattering. The roughly opposite variation tendency of the carrier concentration and the Hall mobility in Figure 3 proves the above analysis, since the carrier density is strongly related to the impurity concentration.[29]

Oxygen vacancies, substitution high valence metallic ions for indium, and H doping are all the important sources of conducting electrons in hydrogenated indium oxide films.[25,30] XPS measurement was carried out to investigate the valence states of Hf and oxygen elements in the IHfO:H films prepared with different H_2concentration. The significant Hf 4f XPS line and the element ratio of Hf/In (3.87±0.04 %, calculated from the XPS peaks) similar to the evaporation target indicate effective and similar Hf doping in all the IHfO:H films (Figure S1). Varying the H_2 concentration during the IHfO:H film deposition does not seem to change the doping effect of Hf elements. According to literature, hydrogen doping enables the replacement of double-electron donors (oxygen vacancy Vo) for single-electron donors (interstitial H_i^+ or substitutional H_O^+)[26,31] and passivation of structural defects,[32] which may reduce the scattering intensity and thus improve the Hall mobility of the TCO films. Thereby, the following discussion will focus on the influence of the H_2 concentration on the oxygen elements.

Posted on 11 Nov 2022 — The copyright holder is the author/funder. All rights reserved. No reuse without permission. — https://doi.org/10.22541/au.166817987.71310189/v1 — This a preprint and has not been peer reviewed. Data may be preliminary.

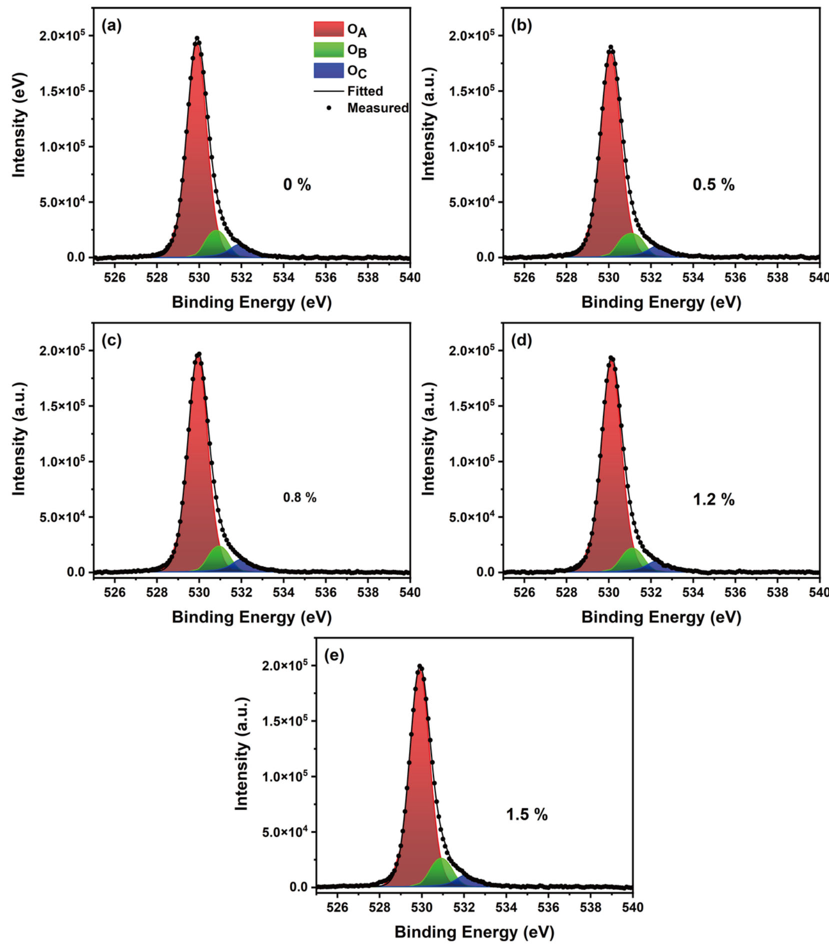

Figure 4 The decomposed O 1s XPS lines of the IHfO:H films deposited with different H_2 concentrations of (a) 0 %, (b) 0.5 %, (c) 0.8 %, (d) 1.2 %, and (e) 1.5 %. All the IHfO:H films were annealed at 200 °C.

Figure 4 illustrates the O 1s core level peaks of the XPS spectra for the IHfO:H films deposited with different hydrogen concentrations. The O 1s XPS lines can be decomposed to three peaks of O_A, O_B, and O_C, with the corresponding binding energies of ˜530.0 eV, ˜531.1 eV, and ˜532.1 eV, respectively. The $O_A$peak with the lowest binding energy of ˜530.0 eV corresponds to the O^{2-} ions in the In_2O_3 lattice. The $O_B$peak at ˜531.1 eV corresponds to the oxygen vacancy Vo. The tiny O_C peak at ˜532.1 eV can be attributed to the hydroxyl bonds appearing in $In(OH)_3$ or InOOH.[27]

It can be seen that, the content of oxygen vacancies ($O_B$peak) in different IHfO:H films shows a slightly decrease as the H_2 concentration increasing from 0 % to 0.8 % and then a rapid increase when the H_2 concentration rises from 1.2 % to 1.5 %. The trend of the oxygen vacancy content varied with the H_2 concentrations is similar to that of the carrier concentration as shown in Figure 3, which demonstrates the influence of H doping on the oxygen vacancy content and thus the carrier concentration. However, a less than 5 % change in oxygen vacancy does not seem to be sufficient to explain the more than 60 % increase in carrier concentration as the hydrogen concentration rises from 1.2 % to 1.5 %. The contribution of hydrogen as a donor to the carrier concentration should also be considered. As mentioned above, hydrogen in TCO films exists in the forms of $H_i^+$and H_o^+. The amount of the interstitial hydrogen H_i^+ can be equated with the amount of hydroxyl ($O_C$peak)[31] which exhibits an increase with increasing the hydrogen concentration

as observed by Huang et al.[27]The sharp rise in the carrier concentration can also be attributed to the sudden rise in the interstitial hydrogen content. In addition, the substitutional hydrogen from the excess hydrogen doping during the deposition would also cause an increase in the carrier concentration.[31]

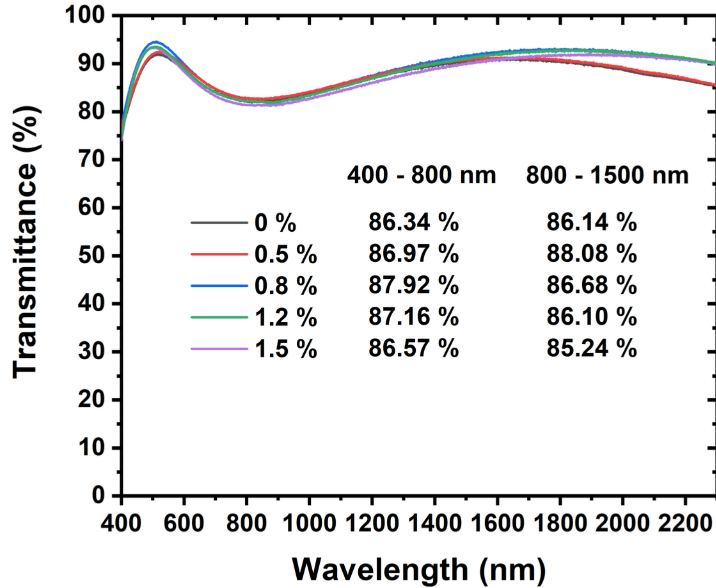

Figure 5 Transmittance in the wavelength range of 400-2300 nm for the IHfO:H films deposited with H_2 concentrations of 0 %, 0.5 %, 0.8 %, 1.2 %, and 1.5 % after post-annealing at 200 in air.

Figure 5 shows the transmittance of the IHfO:H films with different H_2 concentrations in the wavelength range from 400 nm to 2300 nm. The hydrogen concentration does not significantly affect the transmittance of the IHfO:H films in the visible region (400-800 nm) with an average transmittance of ˜87 %. In the NIR region (800-1500 nm), the average transmittance is in the range of ˜85 % to ˜88 %, which is much higher than ˜79 % for the ITO films with the same thickness,[33] thanks to the weaker NIR free carrier absorption (FCA) effect.[34] When the hydrogen concentration is higher than 0.8 %, the average transmittance of the IHfO:H films increases slightly in the range of 1500-2300 nm which, however, is beyond the optical absorption range of crystalline silicon. Considering the application in crystalline silicon solar cells, it can be said that the hydrogen doping concentration (0-1.5 %) hardly effect the optical properties of the IHfO:H films at an annealing temperature of 200 .

According to above experimental results and discussion, adding a decent H_2 gas when depositing IHfO:H films significantly increases the carrier mobility and thus reduces its sheet resistance, but hardly influences the film transmittance. Too much hydrogen can lead to a significant degradation of the electrical properties of the IHfO:H films. Comprehensive consideration of the optical and electrical properties, the optimum H_2 concentration is determined to be 0.8 %.

3.2 The effect of post-annealing on IHfO:H films

Post-annealing is a conventional treatment to improve the crystallinity[28] and to activate the dopants of the TCO films.[35] XRD patterns of the IHfO:H films prepared with 0.8 % H_2 concentration annealed at 100-250 are shown in Figure 6. The XRD pattern of an as-deposited sample is included. Four diffraction peaks of (211), (222), (332), and (444) belonging to In_2O_3 can be determined from the XRD patterns of all the samples. Increasing the annealing temperature does not affect the dominant orientation of the (222) crystal

Posted on 11 Nov 2022 — The copyright holder is the author/funder. All rights reserved. No reuse without permission. — https://doi.org/10.22541/au.166817987.71310189/v1 — This a preprint and has not been peer reviewed. Data may be preliminary.

plane in the IHfO:H films, however, the FWHM of the (222) diffraction peak is significantly reduced and the estimated average grain size increases gradually as depicted in Figure 6. As the annealing temperatures is above 200 °C, the average grain size exceeds 50 nm indicating better crystallinity of the IHfO:H films grown by RPD than that by magnetron sputtering.[19,36] It is worth noting that the as-deposited IHfO:H film is also crystallized in the presence of hydrogen during the deposition. Nevertheless, the as-deposited sample without hydrogen doping is amorphous (Figure S2). That means both post-annealing and hydrogen doping promote the film crystallization.

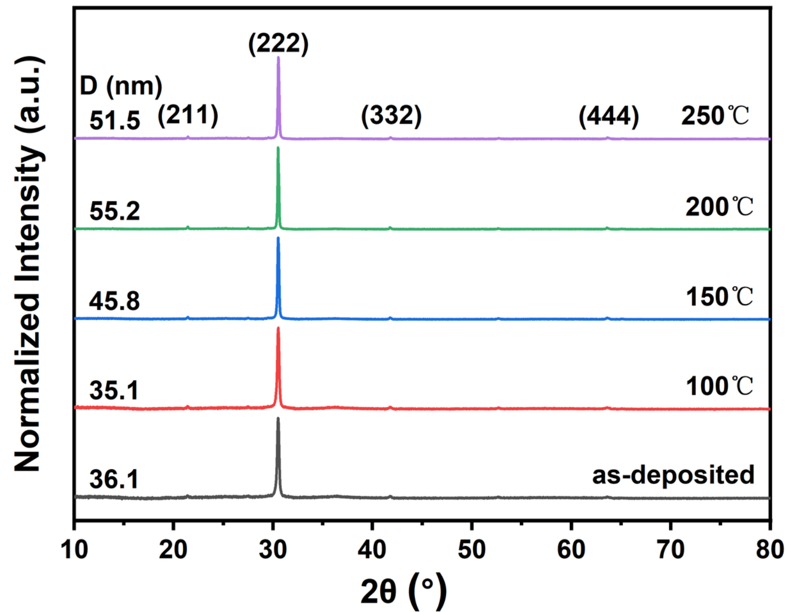

Figure 6 Normalized XRD patterns of the IHfO:H films annealed at different temperatures for 20 minutes. A H_2concentration of 0.8 % was adopted during the deposition.

Figure 7 depicts the annealing temperature dependences of the electrical properties of the IHfO:H films prepared with 0.8 % H_2concentration. The sheet resistance, carrier concentration, and Hall mobility of the as deposited IHfO:H film are 22.39 Ω/, 6.11×10^{20} cm^{-3}, and 41.48 $cm^2V^{-1}s^{-1}$, respectively. When the annealing temperature is lower or equal to 100 °C, no notable changes occur in the electrical properties of the IHfO:H films. The sheet resistance increases slightly as the annealing temperature increasing to 150 °C and then rapidly climbs to 44.97 Ω/ when the annealing temperature reaches 250 °C, which is different from the general observed rule that the sheet resistance of the TCO films decreases with the increase of the annealing temperature.[21,23,25] The following analysis of Hall mobility and carrier concentration varied with the post-annealing temperature will help us understand this phenomenon.

Posted on 11 Nov 2022 — The copyright holder is the author/funder. All rights reserved. No reuse without permission. — https://doi.org/10.22541/au.166817987.71310189/v1 — This a preprint and has not been peer reviewed. Data may be preliminary.

Posted on 11 Nov 2022 — The copyright holder is the author/funder. All rights reserved. No reuse without permission. — https://doi.org/10.22541/au.166817987.71310189/v1 — This a preprint and has not been peer reviewed. Data may be preliminary.

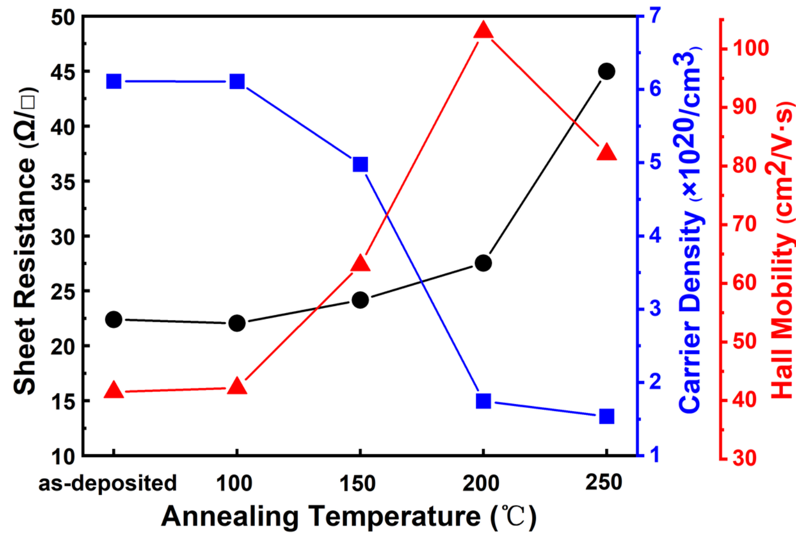

Figure 7 Annealing temperature dependences of sheet resistance, carrier concentration and Hall mobility of the IHfO:H films prepared with 0.8 % H_2 concentration.

As can be seen from Figure 7, the Hall mobility of the IHfO:H films increases rapidly from the as-deposited 41.48 $cm^2V^{-1}s^{-1}$ to 102.92 $cm^2V^{-1}s^{-1}$with an annealing temperature of 200 °C. However, as the annealing temperature is keep increasing to 250 °C, the Hall mobility decreases. The annealing temperature dependence of mobility seems to be consistent with that of the crystallinity, as shown in Figure 6, which implies the possible relationship between the rise of the mobility and the reduced grain boundary scattering.[29] However, the carrier concentration does not increase with the annealing temperature, but shows an opposite tendency as depicted in Figure 7, although it is generally believed that crystallization could promote the activation of dopants.[35] The significant decrease of carrier concentration with annealing temperature, which actually determines the change of sheet resistance, represents the reduced concentration of doping impurity. The weakened ionized impurity scattering and the improved crystallinity together lead to the improvement of the mobility of the IHfO:H films. The slight decrease of the mobility and the average grain size at the annealing temperature of 250 °C are probably related to the escaping of the hydrogen. [34,35]

Posted on 11 Nov 2022 — The copyright holder is the author/funder. All rights reserved. No reuse without permission. — https://doi.org/10.22541/au.166817987.71310189/v1 — This a preprint and has not been peer reviewed. Data may be preliminary.

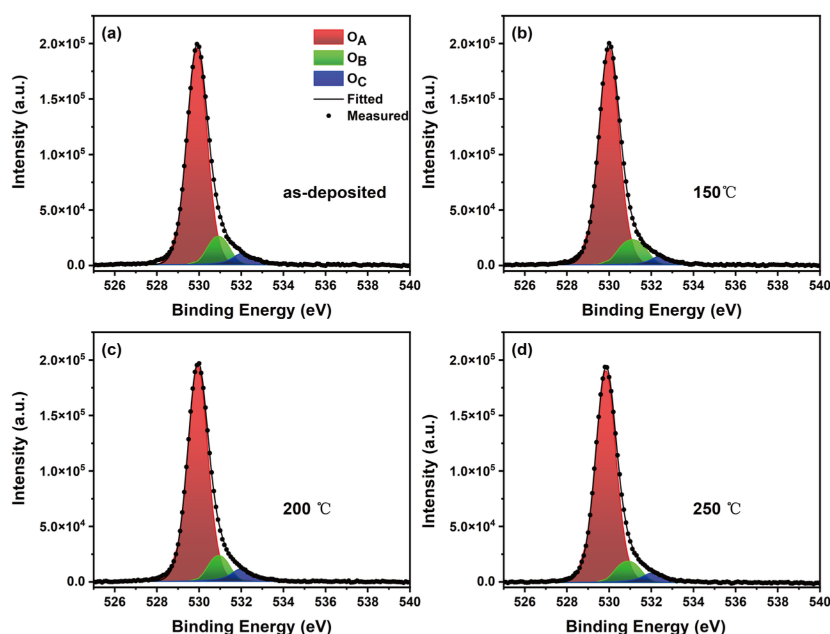

Figure 8 The decomposed O 1s XPS lines of the IHfO:H thin films without annealing (a) and annealed at (b) 150 °C, (c) 200 °C, and (d) 250 °C.

The decomposed O 1s XPS lines of the IHfO:H films annealed at different temperatures are shown in Figure 8. The relative intensities of the three XPS peaks of O_A, O_B, and O_C are listed in Table 2. It can be seen that as the annealing temperature increases to 250 °C, the relative integral area of the O_B peak, representing the oxygen vacancies, gradually decreases from the as-deposited of 13.34 % to 9.74 % due to the filling of the oxygen vacancies by oxygen in the air during the annealing process, as studied by Meng et al.[24] With the same initial Hf and hydrogen doping concentrations, the decrease of the oxygen vacancies is one of the reasons for the decrease of the carrier concentration of the IHfO:H films. In addition, hydrogen might escape during the annealing process as mentioned above, which is another possible reason for the carrier concentration reducing at high annealing temperature. Thereby, the excessively rapid decrease in carrier concentration leads to an increase in the sheet resistance of the IHfO:H films.

Posted on 11 Nov 2022 — The copyright holder is the author/funder. All rights reserved. No reuse without permission. — https://doi.org/10.22541/au.166817987.71310189/v1 — This a preprint and has not been peer reviewed. Data may be preliminary.

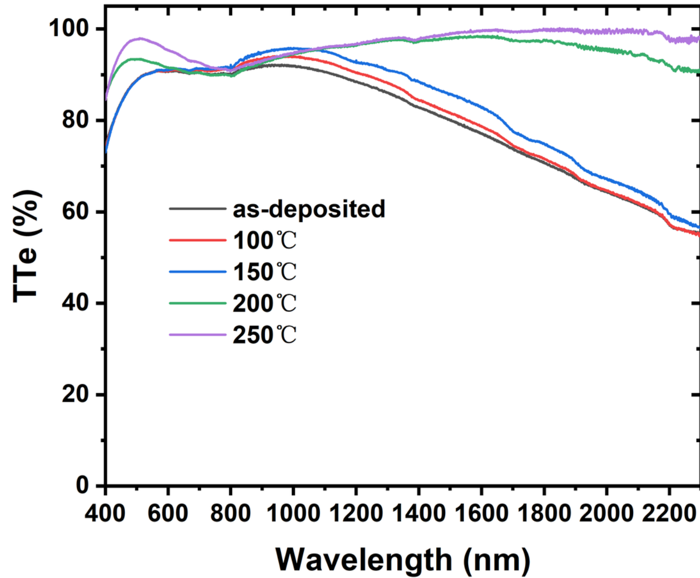

Figure 9 TTe in the wavelength range of 400-2300 nm for IHfO:H films annealed at different temperatures.

As the annealing temperature increases, both the transmission and reflection spectra change significantly due to the change in refractive index caused by the rise in crystallinity (Figure S3).[37] In order to eliminate the effect of reflection on transmission, the effective total transmittance (TTe) spectra are used instead of the transmission spectra to evaluate the optical properties of the IHfO:H films annealed at different temperatures,[38] as shown in Figure 9. TTe is defined as TTe = $\frac{T}{(1-R)}$, where T is the transmittance and R is the reflectance. When the annealing temperature is below or equal to 150 °C, the TTe of the IHfO:H films remains almost unchanged in the visible region while slightly increases in the NIR region. After the annealing temperature increases to 200 °C, the average TTe of the IHfO:H films increases from 88.54 % to 91.16 % in the visible region which can be related to better crystallization with less defects.[39] Meanwhile, the average TTe significantly increased from 77.14 % to 95.61 % in the NIR region. According to the Drude model, FCA is proportional to carrier concentration.[34] Thereby, the IHfO:H films annealed at temperature above 200 °C behave higher transmittance as they have lower carrier concentration as shown in Figure 7.

Overall, the post-annealing treatment shows a significant impact on the crystallinity, the electrical properties, and the optical transmission of the IHfO:H films. Considering the above opto-electronic characteristics comprehensively, the appropriate annealing temperature is about 200 °C which is within the temperature tolerance range of the SHJ solar cells.

3.3 Application of the IHfO:H films on SHJ solar cells

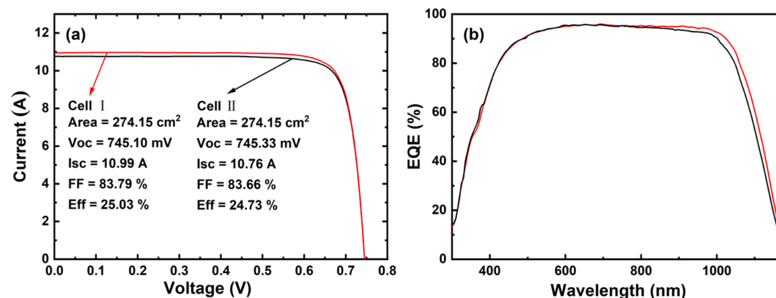

Figure10 (a) The light I-V curves and (b) EQE spectra of the SHJ solar cells with IHfO:H (Cell 1) or ITO (Cell 2) as the front-side TCO under optimal conditions.

Finally, a bifacial SHJ solar cell with an area of 274.15 cm^2 was fabricated using IHfO:H film deposited with a H_2 concentration of 0.8 % as the front-side TCO (Cell I). And a control bifacial SHJ cell with ITO on both sides (Cell II) was also assembled as a comparison. Post annealing was carried out in air under a temperature of 200 °C for 20 minutes for the whole devices. The light I-V and EQE curves of Cell I and Cell II are shown in Figure 10. The two solar cells do not show significant differences in open circuit voltage (V_{oc}) or FF. The improvement of 0.3 % in efficiency (Eff) for Cell I (25.03 %) compared with Cell II (24.73 %) is mainly brought by the increase of 0.84 mA/cm^2 in J_{sc}. The significant increase in EQE in the long wavelength range (>850 nm) indicates reduced FCA for Cell I using IHfO:H compared with Cell I using ITO as the front-side TCO layer. The excellent device performance indicates that the IHfO:H films prepared by RPD have the great application potential in high efficiency SHJ solar cells.

Conclusions

The IHfO:H films (Hf/In ratio=4 % in target, ˜3.87+-0.04 % in the films) with various H_2 concentrations (0-1.5 %) were prepared at room temperature by a low-damage RPD method, followed by post annealing in air atmosphere at different temperatures (100˜250 degC). Under an annealing temperature of 200 degC, the hydrogen concentration hardly changes the crystallinity and the optical properties of the annealed IHfO:H films. The Hall mobility increases from 58.44 $cm^2V^{-1}s^{-1}$ to 102.92 $cm^2V^{-1}s^{-1}$ as the H_2 concentration increases from 0 % to 0.8 % mainly due to the hydrogen doping and the related reduction of the oxygen vacancy concentration. However, higher H_2 concentration of above 0.8% makes the Hall mobility decrease and the carrier concentration increase, which is probably due to the increasing of the interstitial and substitutional hydrogen in the IHfO:H films. Post annealing increases the crystallinity of the IHfO:H films and reduces their oxygen vacancy, causing Hall mobility to rise from 41.8 $cm^2V^{-1}s^{-1}$ to 102.92 $cm^2V^{-1}s^{-1}$and carrier concentration to decrease from 6.11x$10^{20}cm^{-3}$ to 1.75x$10^{20}cm^{-3}$ after 200 degC annealing for the IHfO:H films prepared with optimized 0.8% H_2 concentration. At meanwhile, the average TTe of the IHfO:H films increases from 88.54 % to 91.16 % in the visible region and from 77.14 % to 95.61 % in the NIR region. The significant reduced FCA of the IHfO:H films leads to the long wavelength response improvement in the EQE and 0.84 mA/cm^2 increase in J_{sc} for the SHJ solar cell. An efficiency of over 25% was achieved on the SHJ solar cells using IHfO:H films as the front-side TCO layer.

Acknowledgements

This work was supported by the State Key Program of the National Natural Science Foundation of China (No. 62034001), the Fundamental Research Funds for the Central Universities (No. E0E48919X2 and E1E41804X2), Weiqiao-UCAS Special Projects on Low-Carbon Technology Development (No. GYY-DTFZ-2022-019), and the International Partnership Program of the Chinese Academy of Sciences (211211KYSB20180020).

References

Posted on 11 Nov 2022 — The copyright holder is the author/funder. All rights reserved. No reuse without permission. — https://doi.org/10.22541/au.166817987.71310189/v1 — This a preprint and has not been peer reviewed. Data may be preliminary.

Posted on 11 Nov 2022 — The copyright holder is the author/funder. All rights reserved. No reuse without permission. — https://doi.org/10.22541/au.166817987.71310189/v1 — This a preprint and has not been peer reviewed. Data may be preliminary.

1. De Wolf S, Descoeudres A, Holman Z C, et al. High-efficiency silicon heterojunction solar cells: A review. Green. 2012; 2(1): 7-24. doi:https://doi.org/10.1515/green-2011-0018
2. Louwen A, Van Sark W, Schropp R, et al. A cost roadmap for silicon heterojunction solar cells. Sol Energy Mater Sol Cells. 2016; 147: 295-314. doi: 10.1016/j.solmat.2015.12.026
3. Yoshikawa K, Kawasaki H, Yoshida W, et al. Silicon heterojunction solar cell with interdigitated back contacts for a photoconversion efficiency over 26%. Nat Energy. 2017; 2(5): 1-8. doi: 10.1038/nenergy.2017.32
4. Ru X, Qu M, Wang J, et al. 25.11% efficiency silicon heterojunction solar cell with low deposition rate intrinsic amorphous silicon buffer layers. Sol Energy Mater Sol Cells. 2020; 215: 110643. doi: 10.1016/j.solmat.2020.110643
5. Kim J H, Seong T Y, Ahn K J, et al. The effects of film thickness on the electrical, optical, and structural properties of cylindrical, rotating, magnetron-sputtered ITO films. Appl Surf Sci. 2018; 440: 1211-1218. doi: 10.1016/j.apsusc.2018.01.318
6. Tuna O, Selamet Y, Aygun G, et al. High quality ITO thin films grown by dc and RF sputtering without oxygen. J Phys D. 2010; 43(5): 055402. doi: 10.1088/0022-3727/43/5/055402
7. Sofi A H, Shah M A, Asokan K. Structural, optical and electrical properties of ITO thin films. J Electron Mater. 2018; 47(2): 1344-1352. doi: 10.1007/s11664-017-5915-9
8. Fallah H R, Ghasemi M, Hassanzadeh A, et al. The effect of annealing on structural, electrical and optical properties of nanostructured ITO films prepared by e-beam evaporation. Mater Res Bull. 2007; 42(3): 487-496. doi: 10.1016/j.materresbull.2006.06.024
9. Shi J, Shen L, Meng F, et al. Structural, electrical and optical properties of highly crystalline indium tin oxide films fabricated by RPD at room temperature. Mater Lett. 2016; 182: 32-35. doi: 10.1016/j.matlet.2016.06.084
10. Kim J H, Jeon K A, Kim G H, et al. Electrical, structural, and optical properties of ITO thin films prepared at room temperature by pulsed laser deposition. Appl Surf Sci. 2006; 252(13): 4834-4837. doi: 10.1016/j.apsusc.2005.07.134
11. Haines W G, Bube R H. Effects of heat treatment on the optical and electrical properties of indium-tin oxide films. J Appl Phys. 1978; 49(1): 304-307. doi: 10.1063/1.324386
12. Shigesato Y, Takaki S, Haranoh T. Electrical and structural properties of low resistivity tin-doped indium oxide films. J Appl Phys. 1992; 71(7): 3356-3364. doi: 10.1063/1.350931
13. Clanget R. Ionized impurity scattering in degenerate In_2O_3. Appl Phys. 1973; 2(5): 247-256. doi: 10.1007/BF00889507
14. Bel Hadj Tahar R, Ban T, Ohya Y, et al. Tin doped indium oxide thin films: Electrical properties. J Appl Phys. 1998; 83(5): 2631-2645. doi: 10.1063/1.367025
15. Abe Y, Ishiyama N. Polycrystalline films of tungsten-doped indium oxide prepared by dc magnetron sputtering. Mater Lett. 2007; 61(2): 566-569. doi: 10.1016/j.matlet.2006.05.010
16. Meng Y, Yang X, Chen H, et al. A new transparent conductive thin film In_2O_3: Mo. Thin Solid Films. 2001; 394(1-2): 218-222. doi: https://doi.org/10.1016/S0040-6090(01)01142-7
17. Kobayashi E, Watabe Y, Yamamoto T, et al. Cerium oxide and hydrogen co-doped indium oxide films for high-efficiency silicon heterojunction solar cells. Sol Energy Mater Sol Cells. 2016; 149: 75-80. doi: 10.1016/j.solmat.2016.01.005
18. Wang G H, Shi C Y, Zhao L, et al. Efficiency improvement of the heterojunction solar cell using an antireflection Hf-doped In_2O_3 thin film prepared via glancing angle magnetron sputtering technology. Opt Mater. 2020; 109: 110323. doi: 10.1016/j.optmat.2020.110323
19. Wang G H, Shi C Y, Zhao L, et al. Transparent conductive Hf-doped In_2O_3 thin films by RF sputtering technique at low temperature annealing. Appl Surf Sci. 2017; 399: 716-720. doi: 10.1016/j.apsusc.2016.11.239
20. Meng F, Shi J, Shen L, et al. Characterization of transparent conductive oxide films and their effect on amorphous/crystalline silicon heterojunction solar cells. Japanese J Appl Phys. 2017; 56(4S): 04CS09. doi: 10.7567/JJAP.56.04CS09
21. Zhou Z, Zhang Y, Chen X, et al. Innovative wide-spectrum Mg and Ga-codoped ZnO transparent

conductive films grown via reactive plasma deposition for Si heterojunction solar cells. ACS Appl Energy Mater. 2020; 3(2): 1574-1584. doi: 10.1021/acsaem.9b02064

22. Shi J, Meng F, Bao J, et al. Surface scattering effect on the electrical mobility of ultrathin Ce doped In_2O_3 film prepared at low temperature. Mater Lett. 2018; 225: 54-56. doi: 10.1016/j.matlet.2018.04.102
23. Lu Z, Meng F, Cui Y, et al. High quality of IWO films prepared at room temperature by reactive plasma deposition for photovoltaic devices. J Phys D. 2013; 46(7): 075103. doi: 10.1088/0022-3727/46/7/075103
24. Huang W, Shi J, Liu Y, et al. High-performance Ti and W co-doped indium oxide films for silicon heterojunction solar cells prepared by reactive plasma deposition. J Power Sources. 2021; 506: 230101. doi: 10.1016/j.jpowsour.2021.230101
25. Tark S J, Ok Y W, Kang M G, et al. Effect of a hydrogen ratio in electrical and optical properties of hydrogenated Al-doped ZnO films. J Electroceramics. 2009; 23(2): 548-553. doi: 10.1007/s10832-008-9532-0
26. King P D C, Lichti R L, Celebi Y G, et al. Shallow donor state of hydrogen in In_2O_3 and SnO_2: Implications for conductivity in transparent conducting oxides. Phys Rev B. 2009; 80(8): 081201. doi: 10.1103/PhysRevB.80.081201
27. Huang W, Shi J, Liu Y, et al. Effect of crystalline structure on optical and electrical properties of IWOH films fabricated by low-damage reactive plasma deposition at room temperature. J Alloys Compd. 2020; 843: 155151. doi: 10.1016/j.jallcom.2020.155151
28. Gan T, Li J, Wu L, et al. High carrier mobility tungsten-doped indium oxide films prepared by reactive plasma deposition in pure argon and post annealing. Mater Sci Semicond Process. 2022; 138: 106257. doi: 10.1016/j.mssp.2021.106257
29. Chen M, Pei Z L, Wang X, et al. Intrinsic limit of electrical properties of transparent conductive oxide films. J Phys D. 2000; 33(20): 2538. doi: 10.1088/0022-3727/33/20/304
30. Lee D J, Kim H M, Kwon J Y, et al. Structural and electrical properties of atomic layer deposited Al-doped ZnO films. Adv Funct Mater. 2011; 21(3): 448-455. doi: 10.1002/adfm.201001342
31. Limpijumnong S, Reunchan P, Janotti A, et al. Hydrogen doping in indium oxide: An ab initio study. Phys Rev B. 2009; 80(19): 193202. doi: 10.1103/PhysRevB.80.193202
32. Han C, Yang G, Montes A, et al. Realizing the potential of RF-sputtered hydrogenated fluorine-doped indium oxide as an electrode material for ultrathin SiO_x/poly-Si passivating contacts. ACS Appl Energy Mater. 2020; 3(9): 8606-8618. doi: https://doi.org/10.1021/acsaem.0c01206
33. Addonizio M L, Gambale E, Antonaia A. Microstructure evolution of room-temperature-sputtered ITO films suitable for silicon heterojunction solar cells. Curr Appl Phys. 2020; 20(8): 953-960. doi: 10.1016/j.cap.2020.06.007
34. Koida T, Kondo M, Tsutsumi K, et al. Hydrogen-doped In_2O_3 transparent conducting oxide films prepared by solid-phase crystallization method. J Appl Phys. 2010; 107(3): 033514. doi: 10.1063/1.3284960
35. Koida T, Ueno Y, Shibata H. In_2O_3-based transparent conducting oxide films with high electron mobility fabricated at low process temperatures. Phys Status Solidi A. 2018; 215(7): 1700506. doi: 10.1002/pssa.201700506
36. Shi C Y, Wang G H. Hafnium Oxide and Hydrogen Co-Doped Indium Oxide Films Deposited by Magnetron Sputtering Technology. Adv Mat Res. Trans Tech Publications Ltd. 2021; 1160: 51-55. doi: 10.4028/www.scientific.net/AMR.1160.51
37. Gulen M, Yildirim G, Bal S, et al. Role of annealing temperature on microstructural and electro-optical properties of ITO films produced by sputtering. J Mater Sci Mater Electron. 2013; 24(2): 467-474. doi: 10.1007/s10854-012-0768-8
38. Dong G, Sang J, Peng C W, et al. Power conversion efficiency of 25.26% for silicon heterojunction solar cell with transition metal element doped indium oxide transparent conductive film as front electrode. Prog Photovolt. 2022. doi: 10.1002/pip.3565
39. Zhu F, Huan C H A, Zhang K, et al. Investigation of annealing effects on indium tin oxide

Posted on 11 Nov 2022 — The copyright holder is the author/funder. All rights reserved. No reuse without permission. — https://doi.org/10.22541/au.166817987.71310189/v1 — This a preprint and has not been peer reviewed. Data may be preliminary.

thin films by electron energy loss spectroscopy. Thin Solid Films. 2000; 359(2): 244-250. doi: https://doi.org/10.1016/S0040-6090(99)00882-2

Posted on 11 Nov 2022 — The copyright holder is the author/funder. All rights reserved. No reuse without permission. — https://doi.org/10.22541/au.166817987.71310189/v1 — This a preprint and has not been peer reviewed. Data may be preliminary.

Table 1

Relative intensities of the three XPS peaks of O_A, O_B, and O_C obtained by integrating the peak area of the IHfO:H films with different H_2concentrations.

H_2 concentration [%]	O_A [%]	O_B [%]	O_C [%]
0	83.19	10.81	6.01
0.5	83.03	10.96	6.02
0.8	83.28	10.10	6.61
1.2	83.17	10.17	6.66
1.5	81.52	10.67	7.81

Table 2

Relative intensities of the integral areas of the three XPS peaks of O_A, O_B, and O_C in the IHfO:H films annealed at different temperature.

Annealing temperature [°C]	O_A [%]	O_B [%]	O_C [%]
As-deposited	80.32	13.34	6.33
150	80.16	12.29	6.55
200	83.28	10.10	6.61
250	80.68	9.74	6.57

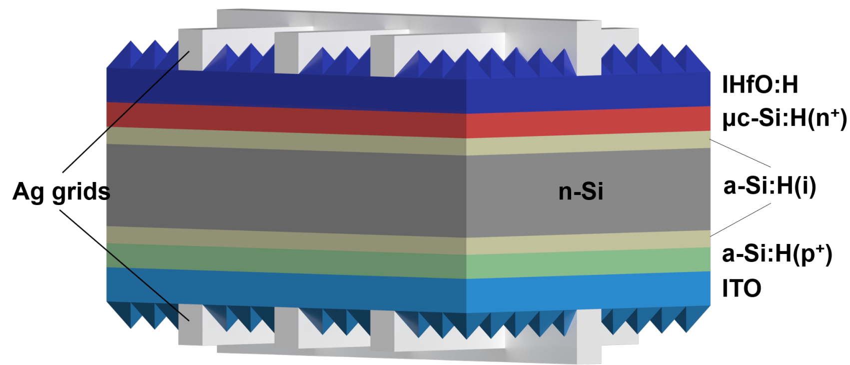

Posted on 11 Nov 2022 — The copyright holder is the author/funder. All rights reserved. No reuse without permission. — https://doi.org/10.22541/au.166817987.71310189/v1 — This a preprint and has not been peer reviewed. Data may be preliminary.

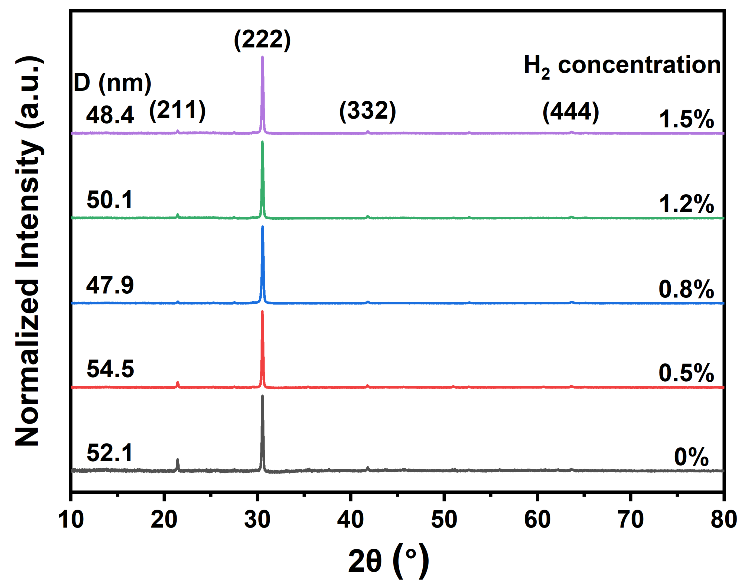

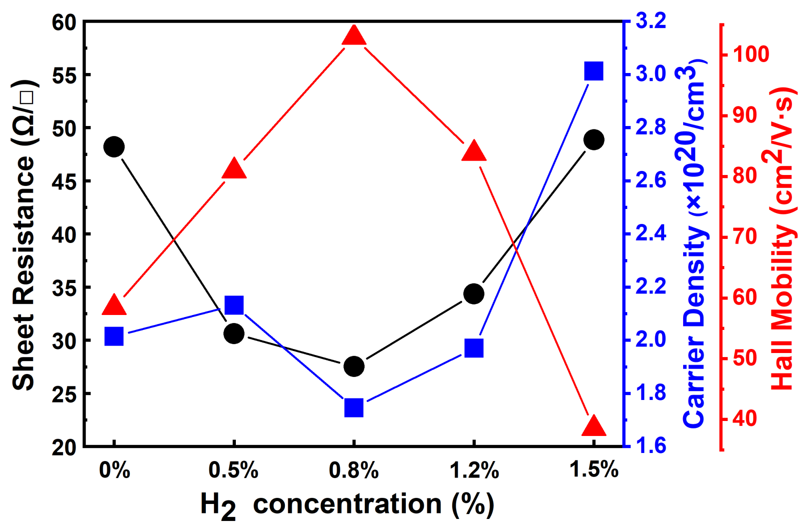

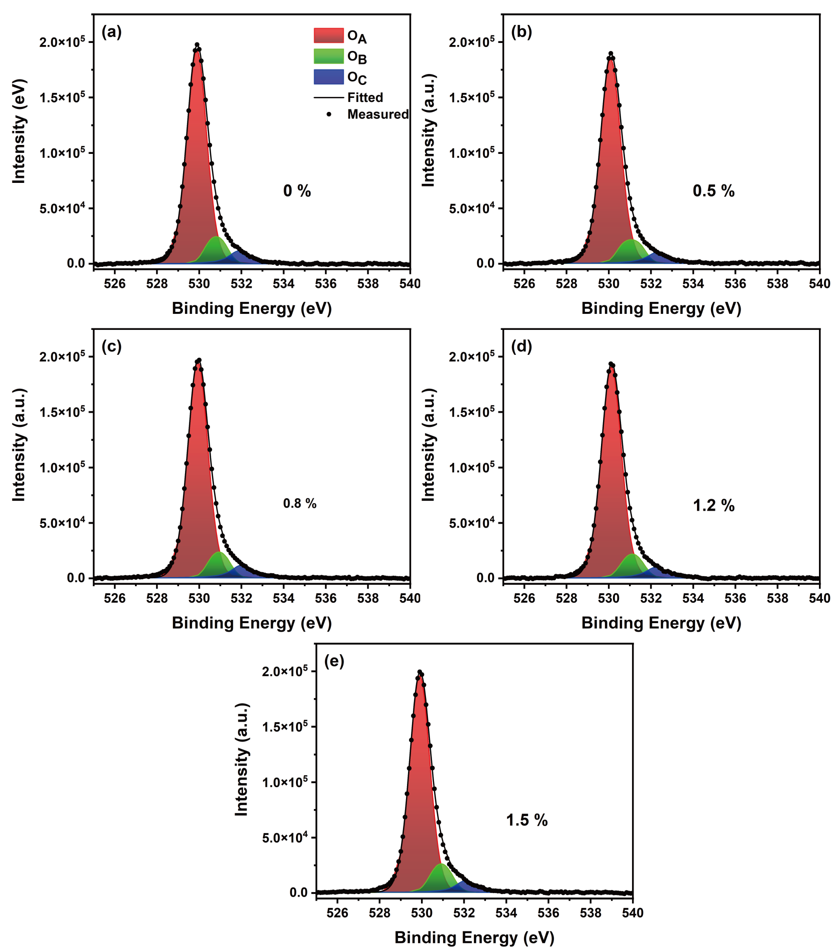

Posted on 11 Nov 2022 — The copyright holder is the author/funder. All rights reserved. No reuse without permission. — https://doi.org/10.22541/au.166817987.71310189/v1 — This a preprint and has not been peer reviewed. Data may be preliminary.

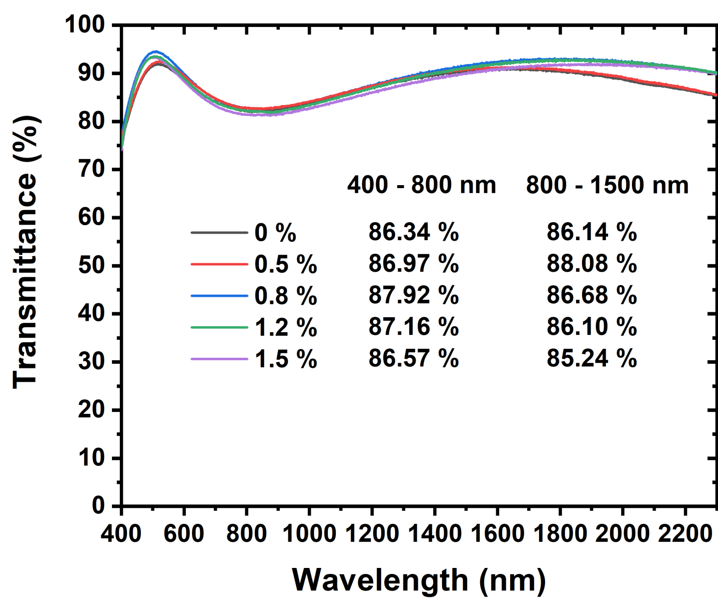

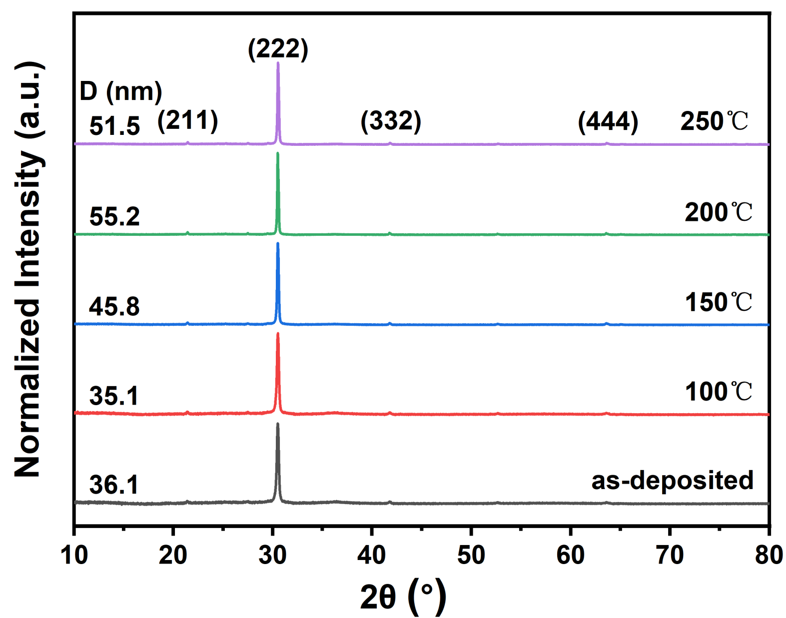

Posted on 11 Nov 2022 — The copyright holder is the author/funder. All rights reserved. No reuse without permission. — https://doi.org/10.22541/au.166817987.71310189/v1 — This a preprint and has not been peer reviewed. Data may be preliminary.

Posted on 11 Nov 2022 — The copyright holder is the author/funder. All rights reserved. No reuse without permission. — https://doi.org/10.22541/au.166817987.71310189/v1 — This a preprint and has not been peer reviewed. Data may be preliminary.

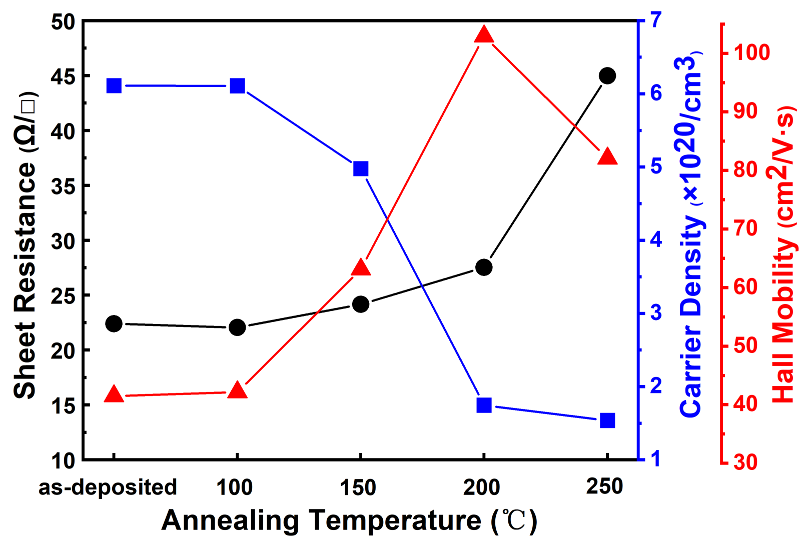

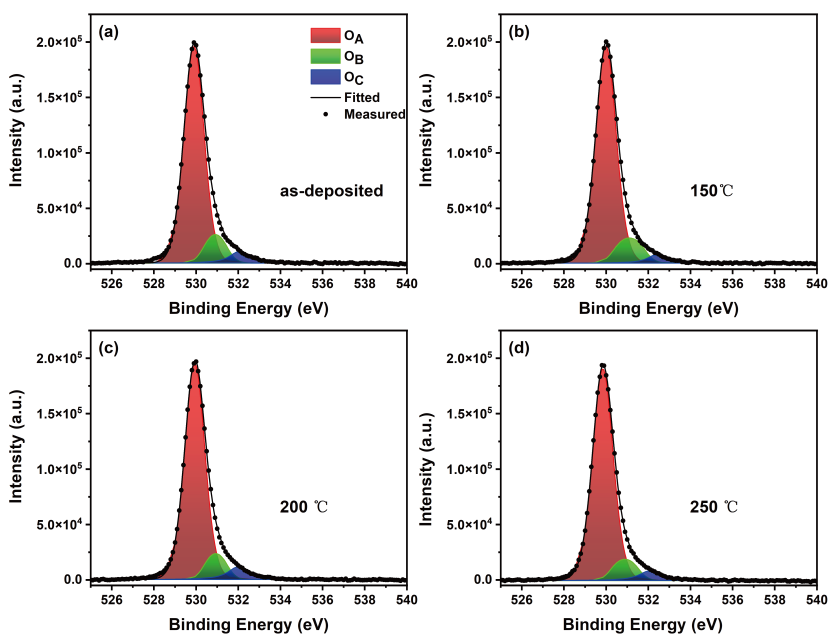

Posted on 11 Nov 2022 — The copyright holder is the author/funder. All rights reserved. No reuse without permission. — https://doi.org/10.22541/au.166817987.71310189/v1 — This a preprint and has not been peer reviewed. Data may be preliminary.